16th World Conference on Earthquake, 16WCEE 2017
Santiago Chile, January 9th to 13th 2017
Paper N° 20202
Registration Code: S-XXXXXXXX

TORSIONAL EFFECTS ON TRANSVERSE LATERAL LOAD RESISTING SYSTEMS

R. T. Leon[(1)], C-H. Fang[(2)]

[(1)] *David H. Burrows Professor, Department of Civil and Environmental Engineering, Virginia Tech, rleon@vt.edu*
[(2)] *Structural Engineer, Building Structures, WSP | Parsons and Brinckerhoff, cfang12@vt.edu*

Abstract

This study focuses on the evaluation of the seismic behavior of transverse lateral load resisting system when the longitudinal load resisting system is subjected to large torsional forces. Two prototype three-dimensional steel structures with three diaphragm types and two different horizontal layouts of the lateral load resisting system were investigated. The structures have symmetric or asymmetric braced frames in the longitudinal direction and moment frames in the transverse direction. Three models of floor diaphragm interactions were considered: a bare steel frame with rigid constraints (*BF+R*); a composite frame with rigid constraints (*CF+R*); and a composite frame (*CF*) without rigid constraints. The structures were subjected to nonlinear static and dynamic analyses under two cases of torsional eccentricity. Case M_{ta_1} represents the conventional accidental eccentricity. Case M_{ta_2} represents the consideration of the bi-axial effects from the two principal directions. The results indicated that (1) the transverse frames show higher strength demands for the asymmetric configuration; (2) the columns in the 1st story in the transverse frames show inelastic behavior for the asymmetric configuration; and (3) The asymmetric structures without rigid diaphragm constraints (*CF*) show the largest increment of both base shear and interstory drift when such structures include the effect of M_{ta_2}.

Keywords: Torsion, diaphragms, analyses, peripheral transverse frames

1. Introduction

In conventional seismic design procedures, such as equivalent lateral force approach (ELF), the strength and stiffness contributions of lateral load resisting systems (LLRS) located perpendicular to the direction being considered are not included. Under this assumption, which is typical of any 2D design approach, the performance of the system is not affected by these transverse systems (henceforth, TS) and is controlled exclusively by the longitudinal system (henceforth, LS). However, for asymmetric structures with ASCE 7-10 [1] horizontal torsional irregularities, the contribution of these TS to the inelastic behavior and collapse resistance of the structures may be significant. These LLRS may provide substantial resistance against the increment of inherent torsion (M_t) and accidental torsion (M_{ta}) in the inelastic range generated by the progressive damage to the major longitudinal LLRS. In addition, the magnitude of torsional resistance also depends on the ability of the diaphragms including slabs, chords and collectors to redistribute forces among the longitudinal and transverse LLRS. Therefore, the in-plane rigidity of diaphragm is another factor influencing the contribution of those transverse peripheral LLRS.

The seismic response for the structures with torsional irregularities has been studied extensively in the past. For locating the center of rigidity (CR) for the 3D structures with rigid diaphragms, Tso [2] presented a simplified plane frame approach which connects these frames with rigid links to the 2D model, so that the story shears of the longitudinal frames can be determined through solving equilibrium equations. Goel and Chopra [3] provided an approach to consider the effect of mass eccentricity without locating the position of C.R. However, these approaches were developed for linear elastic systems with rigid diaphragms.

The nonlinear response of torsional irregular structural system was studied by many researchers. Goel and Chopra [4] implemented a series of analytical studies comparing the dynamic behavior of asymmetric-plan systems with those of symmetric-plan systems. The results indicate that the effect of asymmetric configurations do not affect the response of inelastic systems significantly. Chopra and Goel [5] also compared the ductility and deformation demands in the LLRS of asymmetric systems based on different design provisions. The results show the code-based eccentricity should be modified for the elastic and inelastic systems according to the different levels of inelasticity. De la Llera [6] provided an approach to consider the effect of M_{ta} and predicted the amplified displacement due to M_{ta}. The design forces for structural components can be determined based on the displacements. More recent research has focused on the structural seismic response under the effect of accidental torsion. Erduran and Ryan [7] assessed the seismic behavior of 3D steel braced structures under various hazard levels. The results indicate the response spectrum analyses (RSA) and pushover (or non linear static, henceforth NLSA) analyses are not able to predict the story drift amplified by M_{ta}. DeBock et al. and Jarret et al. [8, 9] discussed the importance of design accidental torsion design provisions in assessing the building collapse capacity. The studies demonstrate the design M_{ta} leads to a significant change of inelastic behavior for structures with high torsional irregularity in nonlinear response history analyses (NLRH). However, none of these research efforts specifically investigated either the contribution of transverse structural systems in both elastic and inelastic stages or the effect of in-plane diaphragm rigidity.

The effect of diaphragm rigidity, as a stand-alone issue, has been the subject of numerous numerical studies [10-13]. The results show the structures with shear walls are influenced by the in-plane rigidity of diaphragm significantly. Basu and Jain [14] presented a superposition-based approach for including the effect of M_t and M_{ta} in the structures with semi-rigid diaphragms. The results show that the strength and ductility demands for the structures with semi-rigid diaphragms are higher than those with rigid diaphragms. De-La-Colina [15] carried out NLRH for a one-story structure with high torsional irregularity. The results show the increment of in-plane diaphragm flexibilities increase the lateral displacement of LLRS by 50%. Fleischman and Farrow [16] presented an analytical model to capture the diaphragm behavior in long-span structures with perimeter LLRS. The difference in the in-plane rigidities may result in unexpected forces and drift patterns in terms of the inelastic behavior. However, these researchers did not discuss the behavior and contribution of the transverse frames perpendicular to the considered earthquake direction.

Transverse frames may provide significant torsional resistance to M_t and M_{ta} in the inelastic range, particularly if the transverse frames are located in the perimeter of the structures. To study this phenomenon, two prototype structures are designed intentionally to comply with different categories of horizontal irregularities based on the definition in ASCE 7-10. The behavior of transverse perimeter frames of these structures is investigated by conducting nonlinear static (NLSA or pushover) and time history (NLRH) analyses in *OpenSEES* [17] under different assumptions of diaphragm rigidity. The variation of interaction of axial force and bending moment (P-M_X-M_Y) in the columns, maximum base shear and roof drift are the three major measurements of the transverse peripheral frame assessed in this study.

2. Systems description

2.1 Design of prototype structures

The 4-story steel prototype steel structures with different configurations used in this study are shown in Fig. 1. Configuration 1 (C1) is for symmetric structures and Configuration 2 (C2) is for asymmetric ones. Both of the configurations have the same seismic weight (8450 kips). In addition, these prototype structures have the same story heights (15 ft. for the 1^{st} story and 12.5 ft. for the 2^{nd} to 4^{th} story) and beam spans (27.5 ft.). In the main direction of loading (Y-dir.), these structures utilize Special Concentrically X-Braced Frames (SCBFs, [18]). Two symmetric transverse perimeter Special Moment Resisting Frames (SMRFs, [18]) provide the lateral resistance in the perpendicular direction (X-dir.). Conventional W-sections with 50 ksi yield strength are used for beam and column members, while rectangular HSS-sections with 46 ksi yield strength are used for brace members. The member sizes are presented in Table 1. In addition, both configurations are designed for a geometry that is just compliant with diaphragms provisions of ASCE 7-10. In particular, the diaphragm aspect ratio (length to width) of 3 is at the upper limit permitted. The slab systems in C1 and C2 are corrugated fully composite floor decks, consisting of 3.0 in. rib and 3.0 in. flat slab with 3.0 ksi normal weight concrete.

ASCE 7-10 uses the concept of a torsional coefficient (TC) to assess torsional irregularity. The torsional coefficient is defined as the maximum story drift divided by the average one, without considering the amplification of accidental torsion. From 3D equivalent lateral load analysis, the torsional coefficients (*TC*) of the diaphragms in each configuration, including the effect of M_{ta}, range from 1.14 to 1.17 for C1 and 1.51 to 1.47 for C2. Based on the definition of ASCE 7-10, C1 belongs to the *no torsional irregularity* category (*TC* < 1.2), and C2 to the *extreme irregularity* category (*TC* > 1.4). The design base shears (V_{design}) corresponding to the SCBFs and SMRFs in C1 and C2 are 0.167W and 0.084W, respectively.

Table 1 – Member sizes for LLRS for C1 and C2

Story	C1			C2						C1/C2	
	SCBFs			SCBFs						SMRFs	
	C1~C4	B1~B4	BR1~BR4	C1,C4	B1,B4	BR1,BR4	C2,C3	B2,B3	BR2,BR3	C5~C8	G1~G3
4^{th}	W12x106	W21x57	HSS5x5x1/2	W12x106	W21x57	HSS6x6x1/2	W12x106	W21x57	HSS6x6x1/2	W14x132	W21x44
3^{rd}	W12x106	W24x76	HSS5.5x5.5x3/8	W12x106	W27x114	HSS7x7x1/2	W12x106	W24x103	HSS7x7x1/2	W14x132	W24x76
2^{nd}	W14x132	W21x57	HSS6x6x1/2	W14x176	W21x73	HSS8x8x5/8	W14x176	W21x73	HSS7x7x5/8	W14x211	W24x84
1^{st}	W14x132	W27x114	HSS7x7x1/2	W14x176	W27x129	HSS9x9x5/8	W14x176	W27x114	HSS8x8x5/8	W14x211	W27x114

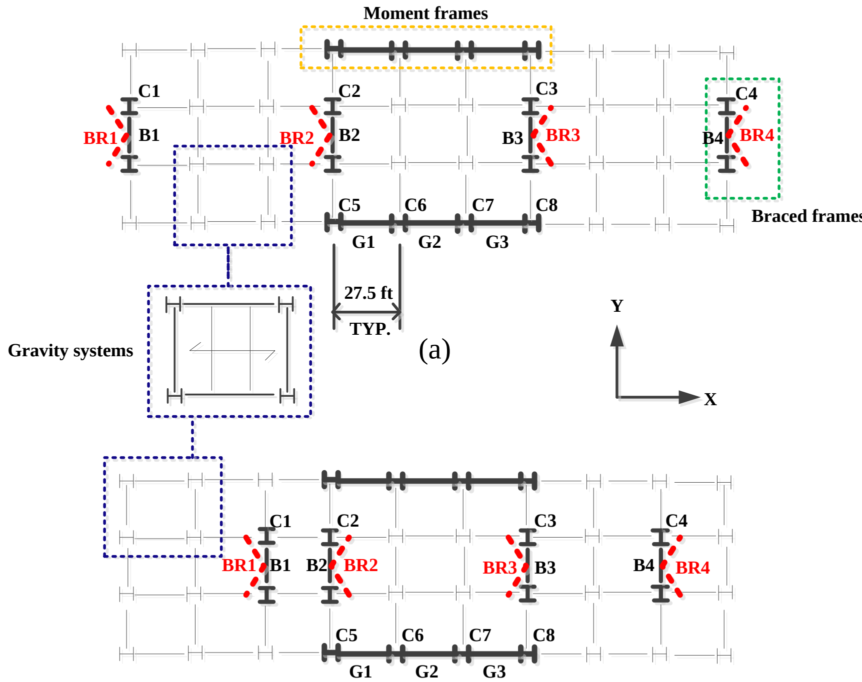

(b)

Fig. 1 – Plan layout of theme structures: (a) C1 and (b) C2

2.2 Site conditions and the selection of ground motions

The design criteria for the prototype structures are taken from ASCE 7-10 and the AISC seismic provision [18]. The structures are assumed to be built at high seismic location on a stiff soil (Site class D, shear wave velocity > 600 ft./sec.)). The mapped acceleration parameters and the corresponding design spectrums are determined as S_s=1.50g and S_1=0.63g, respectively [19].

Seven ground motions selected from PEER NGA data base [20], which is generally consistent with the magnitudes, faults distances, site conditions in the USGS seismic deaggregation data [19], are used in the NLRH. Distance-magnitude pairs of each ground motion are determined by the mean of the disaggregation data corresponding to the 2% probability of exceedence (PE) in 50 years. Table 2 shows the selected ground motions in the study.

Table 2 – Selected ground motions and scaling factors

Ground Motions	PEER NGA ID	Year	Site Class	Magnitude	Fault type
Northridge – 01	1078	1994	D	6.7	Reverse
Imperial Valley - 02	6	1940	D	7	Strike slip
San Fernando	68	1971	D	6.6	Reverse
Loma Prieta	758	1989	D	6.9	Reverse Oblique
Northern Calif - 03	20	1954	D	6.5	Strike slip
Superposition	723	1987	D	6.5	Strike slip
Hollister	23	1961	D	5.6	Strike slip

3. Structural Modeling

The prototype structures are simulated as three-dimensional (3D) finite element models in *OpenSEES* [17]. To reflect the expected yield strengths of steel members, the strength of brace and frame elements is selected as 50 ksi and 55 ksi, respectively. These structural components were simulated by force-based beam column elements consisting of fiber sections with a Menegotto-Pinto material model (*Steel02* in *OpenSEES*). The strain hardening ratios of all steel materials are selected as 0.1%. The buckling of brace is stimulated by a brace imperfection and activation of 2nd order (P-Δ) effects. An artificial imperfection, equal to the 0.1% of effective brace length, is imposed at the middle of each brace. In addition, rigid zone and panel zone models [21] are used for the beam-column joints in the SCBFs and SMRFs, respectively. Reduced beam section (RBS) are used at both ends of the beams in SMRFs. The members in the gravity system were modeled by elastic beam-column elements and their effects accounted for by an including an adjacent frame with the proper masses and with pinned connections.

For the structures with the rigid diaphragm assumption, an in-plane rigid constraint is imposed in each floor to mimic the behavior of infinite in-plane rigidity. In the study, two types of rigid diaphragm structures are investigated: (1) one that includes composite floor action with rigid diaphragm constraints (represented by *CF+R*), and (2) one that utilizes only the bare steel frames with rigid diaphragm constraints (represented by *BF+R*). These two models are used to compare the effects of composite action when the rigid diaphragm assumption is used. For the structures with semi-rigid diaphragms, in-plane deformation is allowed in the diaphragms. The composite frames without rigid diaphragm constraint (represented by *CF*) are used to study the behavior of semi-rigid diaphragm structures. Fig. 2 illustrates the three different assumptions of diaphragm models in this study. The fully-composite slabs with effective width and equivalent thickness are modeled by fiber sections with concrete and steel constitutive models for the beams in the SCBFs and SMRFs. For the beams in gravity systems, the amplification factors for composite actions are applied to the section properties.

In the study, two different combinations of accidental torsion, denoted by M_{ta_1} and M_{ta_2}, are applied in the structures in both NLS and NLRH analyses. M_{ta_1} is used to represent the consideration of accidental eccentricity by shifting the location of diaphragm mass by 5% of the diaphragm dimension perpendicular to the major direction (Y-dir.). M_{ta_2} represents the consideration of bi-axial excitations from both principal directions. The magnitude of the seismic loads along the minor direction is 30% of the seismic loads along the major direction without shifting the diaphragm mass perpendicular to the minor direction (X-dir) [1]. It should be noted that the M_{ta_2} case is not one currently contemplated by codes, although it probably should for self-consistency.

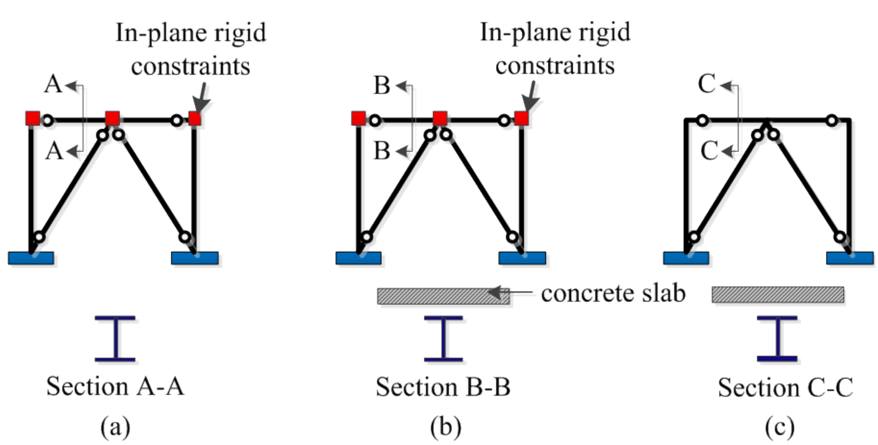

Fig. 2 – Different assumptions for diaphragm simulation: (a) *BF+R*, (b) *CF+R* and (c) *CF*

4. Behavior of SMRFs in the transverse directions

The transverse response of perimeter SMRFs is stimulated by the actions from either M_t or M_{ta}. Fig. 3 illustrates the nomenclature and relationships between the roof lateral displacement and reactions for the longitudinal and transverse direction of the SMRFs in the symmetric (C1) and asymmetric (C2) structures. The reactions and lateral displacement in the transverse direction (Δ_{X1}, V_{X1}) in SMRF1 is defined in Fig. 3

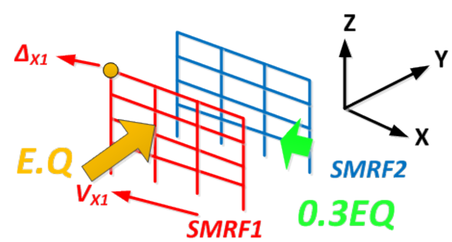

Fig. 3 – Relationships between the roof displacement and base shear in the transverse perimeter SMRF

Fig. 4 illustrates the normalized base shear vs. roof drift (or "pushover curves") of the SMRFs in the transverse direction for the C1 and C2 structures. The magnitudes of base shear and roof drift of pushover curves depend on the change in the magnitude of M_t and M_{ta}. This is influenced primarily by the sequence of inelastic behavior in the SCBFs, such as brace fracture and buckling. For instance, in the C1 structure inelastic action began by buckling of the 3rd story braces in frames BR1 to BR3 (see Figure 1) and the ultimate strength is reached when the 1st story braces in BR1 to BR3 also buckle. A significant increment of diaphragm rotation is observed when this buckling occurs, resulting in large additional forces in the SMRFs along the transverse direction. In other words, the performance of the TS is highly related to the behavior of the LS due to the coupling between the two systems. In Fig.4, note that all quantities in the Y-dir. refer exclusively to the SMRFs; the contributions of the SCBFs and gravity systems to the base shear in the Y-dir. are not included in the figures. In Fig. 4 (a) and Fig. 4 (c), the magnitudes of base shear in the X-dir. (V_{X1}) increase significantly when the structures steps into the inelastic stages (drift ratio of about 0.002). The variation of this increment between the different structural systems (*BF+R*, *CF+R* and *CF*) is due to differences in the sequence of inelastic behavior in the longitudinal SCBFs (i.e. brace buckling and fracture). The change in the lateral stiffnesses of the SCBFs results in the shift of the positions of the CR, which also influences the magnitude of diaphragm torsion resisted by the perimeter SMRFs. The slope of the curves becomes smaller as the NLSA progresses, which corresponds to a smaller rotation increment in the diaphragms. Significant drops of base shear in Fig. 4 (b) and Fig. 4 (d) at drift rations of about 0.015 are caused by the snap back of diaphragm. This phenomenon develops when all of the longitudinal SCBFs reach their ultimate strengths and the large differences in Y-dir. displacement along the length of the structure diminish.

The peak V_{X1} in all structures is significantly higher than the design base shear. The maximum V_{X1} in the C1 structures with semi-rigid diaphragms subjected to either M_{ta_1} or M_{ta_2} shown in Fig. 4 (a) and Fig. 4 (b) are $0.062V_{X1}/W$ and $0.073V_{X1}/W$, respectively. Both are higher than the design base shear of a single SMRF, which is $0.042\ V_{X1}/W$. The corresponding overstrength achieved with respect to the design base shears in the X-dir. are 1.48 and 1.74, respectively. For the C2 structures with semi-rigid diaphragms shown in Fig. 4 (c) and Fig. 4 (d), the peak base shears are $0.069V_{X1}/W$ and $0.081V_{X1}/W$ with an overstrength of 1.64 and 1.93, respectively. These can be compared with an Ω_0 of 2.27 for the single SMRF from the 2D NLSA, indicating that the SMRFs reach 53% to 85% of their ultimate capacity even if the seismic loads are applied only in the perpendicular direction.

These high overstrength factors demonstrate that the rotation of the structures stimulated by asymmetric configurations as well as accidental torsion dominate the performance of the transverse perimeter frames. This also indicates that the SMRFs develop significant inelastic behavior even if the loads are applied only perpendicularly if extreme torsional horizontal irregularities exist in the structure. In addition, the overstrength in the C2 structures is higher than those in C1. This means the asymmetric structures with code-based extreme horizontal irregularities result in higher magnitudes of diaphragm rotation and consequently on higher strength demands in the transverse perimeter frames.

From Fig. 4, one can also observe that the overstrength factors in the structures without rigid diaphragm constraints (*CF*) are higher than those of the other two structures (*BF+R* and *CF+R*). This phenomenon indicates that the perimeter frames may provide more torsional resistance in the 3D analyses when the rigid diaphragm constraints are removed for the asymmetric structures. This is because the transverse lateral displacement of perimeter frames increases due to the diaphragm rotation. The magnitude of rotation in the structures with extremely torsional irregularities is higher than those with typical torsional irregularities in both the elastic and inelastic stages. The structures with semi-rigid diaphragm exhibit larger in-plane deformations when the force redistribution occurs among longitudinal LFRS in the inelastic stages. Therefore, the transverse lateral displacement of the perimeter frames is amplified due to the deformed diaphragm.

These results point out that assuming rigid diaphragm action may not be a conservative assumption for evaluating the behavior of peripheral frames when looking at 3D behavior. This counterintuitive conclusion is the result of inelastic 3D behavior that is difficult to visualize when using conventional 2D linear analysis concepts.

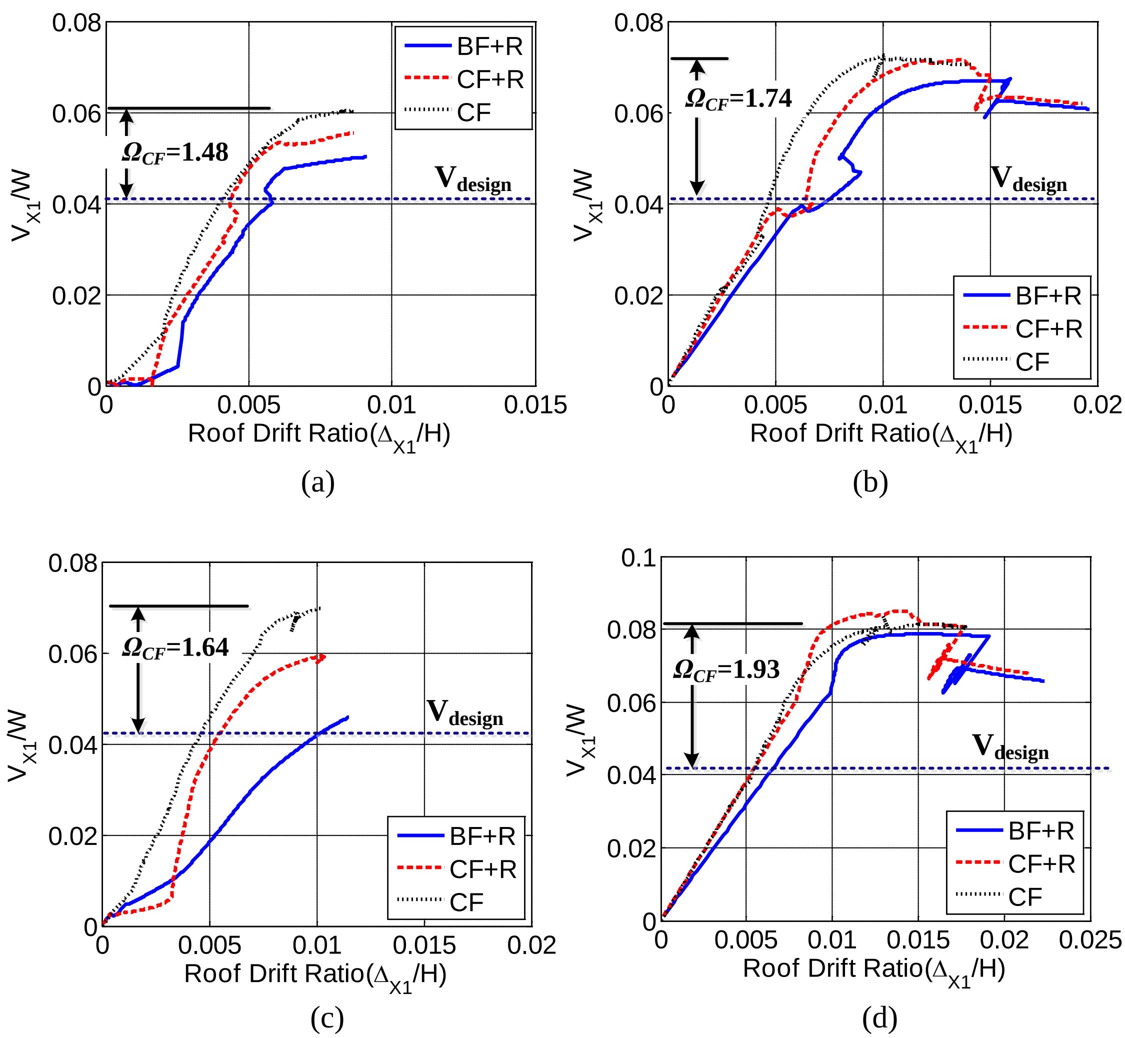

Fig. 4 – Reaction curves for the transverse pheripheral SMRF under different diaphragm assumptions (a) C1 with M_{ta_1} (b) C1 with M_{ta_2} (c) C2 with M_{ta_1} (d) C2 with M_{ta_2}

5. P-M_X-M_Y interaction of corner column

The results of the NLSA indicate that the peripheral SMRFs in the C1 and C2 structures may develop significant inelastic behavior as a consequence of diaphragm rotation. To understand the inelastic behavior of structural components locally, Section *A*, located at the bottom of the left corner column in the SMRF1 in the C2 structure as shown in Fig. 5, is selected as a target section to evaluate the variation of P-M_X-M_Y interaction. Section *A* is assumed as the most critical if structural rotation is considered.

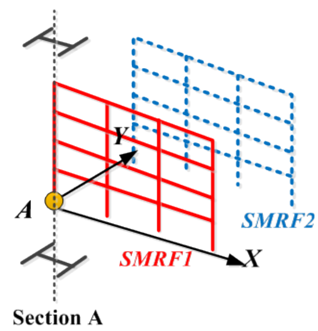

Fig. 5 – Position of selected section for P-M_X-M_Y interaction evaluation

The 3D yield surfaces of Section *A*, including the interaction of axial force and bi-axial bending moment, can be described by Eq. (1) [22]. This equation was determined through a combination of experiments and curve fitting.

$$1.15\left(\frac{P}{P_y}\right)^2+\left(\frac{M_x}{M_{px}}\right)^2+\left(\frac{M_y}{M_{py}}\right)^4+3.67\left(\frac{P}{P_y}\right)^2\left(\frac{M_x}{M_{px}}\right)^2+3.0\left(\frac{P}{P_y}\right)^6\left(\frac{M_y}{M_{py}}\right)^2+4.65\left(\frac{M_x}{M_{px}}\right)^4\left(\frac{M_y}{M_{py}}\right)^2=1.0 \quad (1)$$

where P/P_y is the ratio of the axial force to the squash load, and M_x/M_{px} and M_y/M_{py} are the ratios of the strong and weak axis bending moment to the corresponding expected plastic moment. The nominal strong and weak axis plastic moment capacities of the columns in the SMRFs are amplified by 10% (i.e. R_y=1.10) to the expected plastic moment. The expected plastic moments of Section *A* about strong axis (X-axis) corresponds to the steel strain ranging from 0.18 to 0.20 in the extreme fiber in the section. This strain is governed by the magnitude of M_y, which increases significantly when the inelastic sequences begins.

Fig. 6 illustrates the P-M_X-M_Y interaction for Section *A* in the C2 structures with M_{ta_1} corresponding to the three different diaphragm assumptions. Points A, B and C are used to distinguish the different stages in terms of P-M_X-M_Y interaction in the *CF+R* structures. Points 1, 2 and 3 are used in the *CF* structures.

The interaction curve starts for the *CF* structure at the end of the gravity loading, for which the forces are small ($0.037P/P_y$, $0.0023M_x/M_{Px}$, $0.0023M_y/M_{Py}$). In this curve, Point 1 corresponds to the development of the buckling of the 1st brace in the 3rd story in the SCBF, and Points 2 to 3 correspond to the buckling of the braces in BR1 to BR3 in the 1st story, in sequence. The brace buckling in the 1st story leads to the significant increment of diaphragm rotation and results in similar magnitudes of M_x/M_{px} and M_y/M_{py} in Section *A* (i.e. Points 2 and 3). Point 3 corresponds to the brace fracture in the 3rd story for BR1, which results in a decrease of M_x/M_{px} in the column. The variation of P-M_X-M_Y interaction of *CF+R* is also shown in Fig. 6. A significant increment of M_y can be observed after Point B due to the simultaneous buckling of three braces in the 1st story in BR1 to BR3. Therefore, the sharp increment of M_y that develops in Section *A* is caused directly by the severe rotation of the diaphragm. This phenomenon results in the difference in slopes of P-M_X-M_Y interaction between *CF* and *CF+R* after Point 1 and B. In addition, after Point 3 and C, the section capacity is fully developed corresponding a significant section inelasticity.

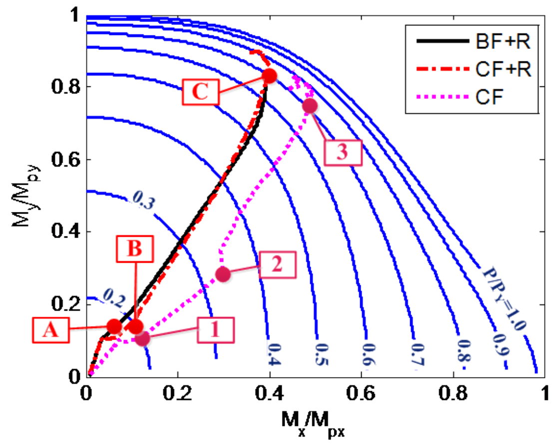

Fig. 6 – P-M_X-M_Y interaction of Section *A* in C2 with M_{ta_1}

6. Dynamic response for peripheral transverse moment frames

Non-linear time history analyses are used to investigate the dynamic behavior of the perimeter transverse moment frames (i.e. SMRF1) in the C1 and C2 structures with the inclusion of M_{ta_1} and M_{ta_2} under different assumptions of diaphragm rigidities. The relationships between peak base shear ratios and maximum roof drift ratios in the X-dir. are represented in Table 3. For all structures, the increment of reaction ratios is significant due to the bi-axial effect (i.e. M_{ta_2}). For instance, the average base shear of the *CF*-C2 structure increases from 0.0351 to 0.0615V_{X1}/W, which is higher than the design base shear (V_{design}) of 0.042 V_{X1}/W for a single SMRF. The phenomenon shows the inclusion of bi-axial excitation significantly increases the reaction magnitudes in the transverse perimeter frames of symmetric and asymmetric structures.

The C2 structures without rigid diaphragm constraints (*CF*) exhibit the largest magnitude of $(V_{X1}/W)_{max}$. The ratios of the *BF+R*, *CF+R* and *CF* structures with M_{ta_2} are 0.0484, 0.0561 and 0.0615, respectively. However, in the C1 structures, the corresponding ratios under the three diaphragm assumptions are 0.0607, 0.0598 and 0.0600. The ratios of C1 and C2 structures with rigid diaphragm are higher than those with semi-rigid diaphragm. This result indicates the inclusion of in-plane rigidity of diaphragm results in a significant decrease of the magnitude of the reaction.

The in-plane rigidity of diaphragm significantly influences the magnitude of maximum roof drift ratio along the transverse direction [$(RDR_{X1})_{max}$] of SMRFs in the C2 structures subjected M_{ta_2}. The *CF* structure exhibits the largest $(RDR_{X1})_{max}$ among the three diaphragm assumptions caused by the removal of rigid constraints. For the structures with M_{ta_1}, however, the influence in terms of roof drift among the structures with different diaphragm assumptions is not as significant as those with M_{ta_2}.

Table 3 – Peak reactions ratios vs. roof drift ratios

MCE		*BF+R*		*CF+R*		*CF*	
		M_{ta_1}	M_{ta_2}	M_{ta_1}	M_{ta_2}	M_{ta_1}	M_{ta_2}
C1	$(V_{X1}/W)_{max}$	0.0284	0.0607	0.0300	0.0598	0.0306	0.0600
	$(RDR_{X1})_{max}$	0.0035	0.0081	0.0035	0.0070	0.0034	0.0067
C2	$(V_{X1}/W)_{max}$	0.0309	0.0484	0.0318	0.0561	0.0351	0.0615
	$(RDR_{X1})_{max}$	0.0028	0.0059	0.0027	0.0054	0.0032	0.0068

7. Conclusions

The analyses in this study are limited to low-rise structures with longitudinally braced systems and transverse perimeter moment frames. In the study, the results from non-linear static analysis indicate that the contribution of transverse perimeter moment frames to the lateral resistance of entire systems is significant after the braced system develops its ultimate strength. The contributions to the lateral resistance from the moment frames is provided by a combination of the (1) torsional resistance due to the high coupling effect between transverse and longitudinal frames and (2) minor bending of columns of peripheral frames. Based on the analytical results, the peak base shear ratios in the peripheral moment frames in the transverse direction in the asymmetric structures are significantly higher than the design base shear of the moment frames regardless of the assumptions of in-plane diaphragm stiffness and the types of accidental torsion. This demonstrates that these frames would have higher lateral strength demands in both symmetric and asymmetric structures when the ground excitations are introduced in the longitudinal direction. This also indicates the inelasticity of the transverse perimeter frames may provide a significant contribution in the entire 3D system due to the coupling behavior between transverse and longitudinal frames. The current overstrength factors and response modification factors used for designing the 3D structures need to be reevaluated.

The analytical results show the removal of rigid diaphragm constraint leads to higher magnitudes of peak base shear and roof drift in the peripheral transverse frames, especially for the asymmetric structures with code-based extremely torsional irregularities. The diaphragm rotation and the in-plane diaphragm deformation both amplify the lateral displacement of frames in the transverse direction. However, the phenomenon is not significant in the structures with typical torsional irregularity. This indicates the in-plane rigidity of diaphragm provides a stronger lateral constraint on the peripheral transverse frames in the asymmetric structures. Therefore, the adjoining structural members to the transverse frames in the semi-rigid diaphragms, such as collectors and chords, have a higher demand on axial strength.

Columns in the transverse peripheral frames develop significant inelastic behavior for the asymmetric structures companying with the increment of diaphragm rotation. This inelasticity is developed at the base of the column due to the effect of bi-axial bending from the seismic loads as well as diaphragm rotation. This demonstrates the inelasticity may develop at the bases of the columns in the transverse peripheral frames before the first member failure in the longitudinal frames.

8. Acknowledgements

The financial support of the Via Department of Civil and Structural Engineering at Virginia Tech is gratefully acknowledged.

9. Copyrights

10. References

[1] American Society of Civil Engineers (2010): *Minimum Design Loads For Buildings and Other Structures ASCE 7-10*. American Society of Civil Engineers. Reston, VA.

[2] Tso W.K. (1990): *Static eccentricity concept for torsional mement estimations*. Journal of Structural Engineering, ASCE **116**(5), 1199-1212.

[3] Goel R.K. and Chopra A.K. (1993): *Seismic code analysis of building without locating centers of rigidity*. Journal of Structural Engineering, ASCE **119**(10).

[4] Goel R.K. and Chopra A.K. (1991): *Effects of plan asymmetric in inlelastic seismic response of one-story systems*. Journal of Structural Engineering **117**(5).

[5] Chopra A.K. and Goel R.K. (1991): *Evaluation of torsional provision in seismic codes*. Journal of Structural Engineering **117**(12).

[6] De la Llera J. C. and Chopra A.K. (1994): *Estimation of accidental torsion effects for seismic design of buildings*. Journal of Structural Engineering **121**(1).

[7] Erduran E. and Ryan K. L. (2011): *Effects of torsion on the behavior of peripheral steel-braced frame systems*. Earthquake Engineering and Structural Dynamics **40**, 491-507.

[8] DeBock D. J., et al. (2013): *Importance of seismic design accidenal torsion requirements for building collapse capacity*. Earthquake Engineering and Structural Dynamics **43**(6), 831-850.

[9] Jarrett J.A., et al. (2014): *Accidental torsion in nonlinear response history analysis*. Tenth U.S. National Conference on Earthquake Engineering. Anchorage, Alaska.

[10] Moon S.K. and Lee D-G. (1992): *Effects of inplane floor slab flexibility on the seismic behaviour of building structures*. Engineering Structures **16**(2).

[11] Saffarini H.S. and Qudaimat M.M. (1992): *In plane floor deformations in RC structures*. Journal of Structural Engineering ASCE **118**(11), 3089-3102.

[12] Tena-Colunga Arturo and Abrams Daniel P. (1995): *Simplified 3-D dynamic analysis of structures with flexible diaphragms*. Earthquake Engineering and Structural Dynamics **24**, 221-232.

[13] Ju S. H. and Lin M. C. (1999): *Comparison of building analysis assuming rigid or flexible floors*. Journal of Structural Engineering ASCE **125**, 25-31.

[14] Basu D. and Jian S.K. (2004): *Seismic analysis of asymmetric buildings with flexible floor diaphragms*. Journal of Structural Engineering **130**(8).

[15] De-La-Colina (1999): *In-plane floor flexibility effects on torsionally unbalanced systems*. Earthquake Engineering and Structural Dynamics **28**, 1705-1715.

[16] Fleischman R. B. and Farrow K. T. (2001): *Dynamic behavior of perimeter lateral-system structures with flexible diaphragms*. Earthquake Engineering and Structural Dynamics **30**, 745-763.

[17] Pacific Earthquake Engineering Reaserch Center (2013): OpenSEES.

[18] American Institute of Steel Construction (2010): *Seismic Provisions for Structural Steel Buildings, ANSI/AISC 341-10*. American Institute for Steel Construction. Chicago, IL.

[19] U.S. Geological Survey (2014). http://www.usgs.gov/.

[20] Pacific Earthquake Engineering Research Center (2014). http://peer.berkeley.edu.

[21] F.A. Charney and W. M. Down (2004): *Modeling procedures for panel zone deformations on momnet resisting frames. Connections in Steel Structures V*. Amsterdam.

[22] Orbison James G., et al. (1982): *Yield surface applications in nonlinear steel frame analysis*. Computer methods in applied mechanics and engineering **33**, 557-573.